ANALYSIS OF EFFECTS AFTER TYPHOON 8115 IN COASTAL AREA AND FIELDS IN HOKKAIDO, NORTHERN JAPAN, USING LANDSAT MSS DATA

Shigetsugu UEHARA
National Research Center for Disaster Prevention,
Science and Technology Agency(STA)
3-1 Tennodai, Sakura-mura, Niihari-gun,
Ibaraki-ken 300-12, Japan

Kiyoshi TSUCHIYA
Chiba University
1-3 Yayoicho, Chiba-shi, Chiba-ken 280,
Japan

Yuichi YAMAURA & Kazuo TACHI
Earth Observation Center(EOC),
National Space Development Agency of Japan(NASDA)
Ohashi, Hatoyama-mura, Hiki-gun,
Saitama-ken 350-03, Japan

Abstract

Based on Landsat MSS data taken consecutively after typhoon 8115 which brought heavy rainfall over Hokkaido and subsequent flood, coastal phenomena and feasibility of detecting flooded area were investigated assisted with areal photos taken immediately after the previous flood.

It was found there exist fairly complicated meso-scale phenomena such as counter currents along the coast of eastern Hokkaido. In a small bay the existence of local circuration generated perhaps due to the effect of coastal shape and ocean current was observed also.

Several experiments reveal that MSS band 4 and 5 imageries are effective to detect sea surface phenomena.

Detecting flooded area in mid-eastern plain of Hokkaido was fairly difficult from the MSS imagery analysis.

I. Introduction

Recently the utilization of remotely sensed data by satellites has been increasing year by year and a lot of papers have been published in many countries including Japan.

Tsuchiya, one of the authors, et al.[1] indicated examples of sea surface phenomena around Japan revealed by airborne MSS, Landsat MSS, Landsat RBV and Geostationary Geometrological Satellite of Japan(GMS) data.

Regarding sea surface phenomena, Munday et al.[2] reported about the detection of oil slicks and oil spill by MSS and MSC. In 1980, Ochiai reported the effectiveness of airborne MSS and Landsat RBV camera in the detection of oil slicks in coastal area in Japan [3]. As early as 1973, Pirie et al.[4] and Klemas et al.[5] studied suspended substances and coastal processes based on Landsat MSS data. As to oceanic front, Mun and Gordon[6] carried out a fine study based on Landsat MSS data, while Pierson et al.[7] made a good analysis based on Landsat MSS and SKYLAB EREP data.

For the detection of expanding patterns of river effluents from the river, Tsuchiya et al.[8] reported a result of digital analysis around Ishikari Bay in Hokkaido based on Landsat MSS and

Landsat RBV camera data.

In this paper, indicated are water surface phenomena near the coast and effects in not only coastal area but also fields after Typhoon 8115 which landed in Hokkaido, northeast one of four main islands of Japan, on August 23 in 1981. In the analysis of the phenomena and the effects, Landsat MSS data of August 25, two days after the typhoon,were mainly utilized.

The water surface phenomena and the effects in coastal area concerned are on a front of muddy river water in the sea, counter currents to the ocean current, bay current variation in a small bay and a clear water flow through a swamp into a muddy lake.

II. Analysis of Coastal Phenomena as Revealed by MSS Data

It is recognized that in the imageries of Landsat MSS band 4 and 5 of August 25, radiance of sea water near the coastal line is greater than those of September 30, 1981 and the high radiant area is much more widespread(See Photo 1 and 2). The high radiant pattern in the coastal area is thought to be mostly muddy river water into the sea after the heavy rainfall caused by Typhoon 8115.

The following four phenomena are observed in Landsat MSS imageries of August 25 and also of September 30;

A front of muddy water 10 to 35 kilo-meters at sea along the coastal line
Water flows along the coast of the Tokachi Plain(Indicated in Fig.1) and mixing with the flows of the opposite direction near Kombumori(Indicated in Fig.1 also)
Muddy water pattern in Akkeshi Bay(Indicated in Fig.1) suggesting clockwise flows
Water flows into Lake Akkeshi at the river mouth

The results of analtsis of phenomena listed above are described in the following paragraphs.

II.1 Front of Muddy Water

According to the sea truth data, a sharp change of salinity from 24 ‰ to 32 ‰ takes place at off the mouth of the Tokachi River (Indicated in Fig.1) where deapth is in the range from 50 to 120 meters(See Fig.2 and 3).

Also according to the measurement data of water volume of the Tokachi River at the points A and B(indicated in Fig.1), water amount of the river remarkably increased on 23 and 24 of August(See Fig.4).

Judging from the two facts above, the pattern of water is considered to be that by rivers in the Tokachi Plain.

It is recognized from the imageries of MSS band 4 of August 25 that a front of muddy water coincides with the iso-line of around 200 meters' depth(Photo 1 and Fig.2).

On the other hand, the front of muddy water on September 30 approximately coincides with a 70 meters depth contour line. Therefore the front of muddy water move forward or backward in accordance with volume of discharged river water into the sea, where an ocean current must have some effect on the formation of the front.

II.2 Water Flows along Coast

The ocean current flows from northeast to southwest off both Akkeshi Bay and the coast of the Tokachi Plain(See Fig.5). On the other hand, the water flows around the river mouth prove that the direction of current along the coast near the Tokachi Plain is from southwest to northeast. Therefore a meso-scale counter current is

thought to exist as is shown by a thick arrow in Fig.5, and it is observed in MSS band 4 imagery on August 25 that the current from southwest along the coast mixes with that from northeast near Kombumori(See Photo 1).

II.3 Bay Current

Clockwise rotation of muddy water in Akkeshi Bay is recognized in MSS imageries on both August 25 and September 30. Especially, extremely muddy water rotation is observed in the former imagery.

Multi-temporal comparison of Landsat MSS data shows the feature of water flows change according to tide or season(Photo 3). In winter, water in the bay is clearer, and the flowing pattern of ice there is obviously different from that of muddy water in summer. Bay current is considered to be affected by the ocean current off Akkeshi Bay.

II.4 Clear Water Flowing into Lake

According to MSS band 4 and 5 imageries on both August 25 and September 30, relatively clear water flowing into Lake Akkeshi(Indicated in Fig.1), while the lake is not clear owing to high plankton density (See Photo 3 (a) and (b)). Water of the river is not muddy even immediately after the typhoon though that of other rivers contain plenty of mud.

III. Detection of Flooded Area

An attempt was made to detect the flooded area in the Tokachi Plain from Landsat imageries taken two days after Typhoon 8115 which passed over Hokkaido on August 23 and caused flood in the area.

Unfortunately the area in the MSS imageries taken before the flood were entirely covered with cloud, so the scenes which were applicable to the analysis were only those of August 25 and September 30, 1981 after the flood was over.

It was not easy to detect the flooded area due to the following reasons;

a) The flood caused by Typhoon 8115 was not so great.
b) The surface condition changed between August 25 and September 30, which makes multi-temporal analysis difficult. For example, at the beginning of September a spring wheat farm, where wheat was reapt at the end of July, was digged, and potatoes were cropped for crop rotation almost at the beginning of September.
c) A part of the area concerned was covered with thin cloud which makes digital analysis difficult.

To clear the difficulties above, color areal photos(Photo 6 and 7) were greatly effective. The photos were taken not after Typhoon 8115 but on around August 7, four days after previously passed Typhoon 8112 which caused great and widespread flood in Hokkaido. There is a good reason to assume that flooded area by heavy rainfall of the previous typhoon may be flooded again by the rainfall of the present typhoon, Typhoon 8115. Thus it is reasonable to make use of the areal photos taken on around August 7, 1981.

In fact, correspondence of traces of submergence between areal photos and Landsat MSS false color images(band 4, 5 and 7) was recognized(See Photo 5 and 7).

The analized areas are shown in Fig.1 and Photo 4 and 5.

Using Landsat digital image data analysis system, the spectral characteristics(See Fig.6) of the sites interpreted as flooded area (See Photo 5) in Landsat image on August 25 were computed and the flooded area was classified.

IV. Concluding Remarks

The forgoing analysis indicates the followings;

i) Landsat Mss band 4 and 5 black-and-white imageries, including two-band composite false color imageries (e.g. blue and green for band 4 and red for band 5), are effective for the detection of meso-scale coastal phenomena such as a front of muddy river water discharged into the sea, a counter current near a coast, bay current variation in a small bay and clear water flows into a muddy lake.

ii) Small-scale flood in fields, such as less than a few hundred square meters in area, can be detected. Especially, MSS false color imageries(blue, green and red for band 4, 5 and 7 respectively) and the color areal photos after flooding were valid in the analysis.

Acknowledgements

The authors are grateful for the useful technical advices of Hon.Prof.S. Genda and Prof.T.Miwa of Chiba University and Ms.T.Satoh of National Research Center for Disaster Prevention, STA and for the efforts to provide us with valuable data and informations of Messrs.Y.Kume, M.Kikuchi and T.Ishiwata of Hokkaido Development Agency, Mr.S.Kurashina of Maritime Safty Agency, Mr.K. Kitano of Fisheries Agency, Mr.T.Kobayashi of Kushiro Fishery Experiment Station, Mr.J.Ogasawara of Wakkanai Fishery Experiment Station and Mr.M.Kanahashi of Akkeshi Fishery Co-operative Society.

The authors' deep appreciation is due to Messrs.A.Tsuda and Y.Yamamoto of EOC/NASDA for their support and Mr.T.Okabe et al. of Remote Sensing Technology Center, Messrs.T.Fukuda and C.Ishida of EOC/NASDA for their technical aids.

References

[1] Tsuchiya K., Application of remotely sensed data to the detection of sea surface phenomena, Acta Astronomica Vol.8, No.5-6, pp.497-509, 1981.

[2] Munday Jr.J.C., McIntyre W.G. and Penny M.E., Oil slick studies using photographic and multispectral scanner data, Proc. 7th Int. Symp. on RS of Environment, 1027, ERIM, 1971.

[3] Ochiai H., Application of multi-spectral data to the detection of sea surface phenomena, Abstract, COSPAR, 23rd Plenary Meeting, including seven symposia, two workshops and topical sessions, p.335, COSPAR, 1980.

[4] Piries D.M. and Steller D.D., California coastal study, NASA SP-351, 1413, 1973.

[5] Klemas V., Otley M. and Rodgers R., Monitoring coastal water properties and current, NASA SP-351, 1387, 1973.

[6] Mund G.A. and Gordon H.R., Relationships between ERTS radiances and gradiances across ocean fronts, NASA, SP-351, 1279, 1973.

[7] Pierson W.J., Marlatt W.E., Byrns Z.H. and Johnson W.R., Ocean and atmosphere, NASA SP-399, 221-228, 1978.

[8] Tsuchiya K., Ochiai H. and Takeda K., Application of Landsat data in the study of oceanographic environment, Proc. 5th Canadian Symp. on RS pp.464-477, 1978.

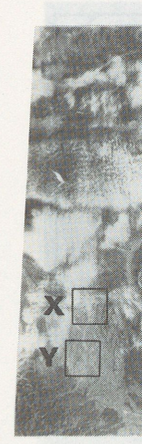

Photo 1 L

Photo 2

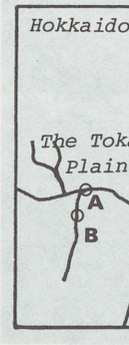

Fig.1 Ma
Note: A
w
F

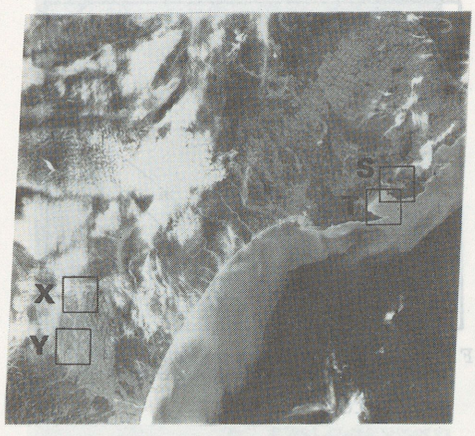

(a) Band 4

(b) Band 5

Photo 1 Landsat MSS imageries of eastern part of Hokkaido (WRS path 114 and row 30) on Aug. 25, 1981

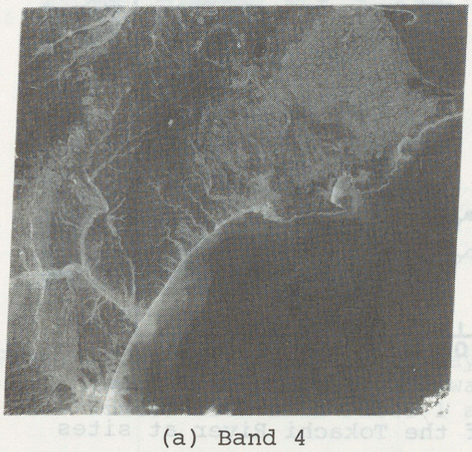

(a) Band 4

(b) Band 5

Photo 2 Landsat MSS imegeries of eastern part of Hokkaido (WRS path 114 and row 30) on Sep. 30, 1891

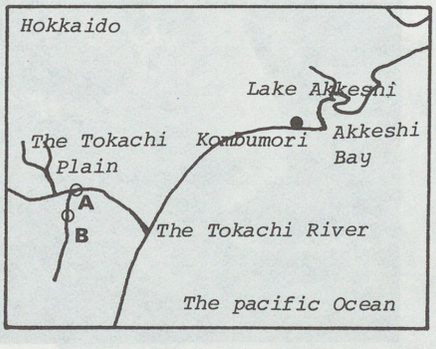

Fig.1 Map of eastern Hokkaido
Note: A & B; Sites of river water measurement (See Fig.4)

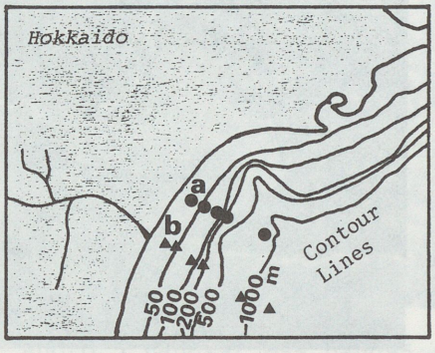

Fig.2 Contour map of sea depth
Note: a & b ; Sites of salinity measurement (See Fig.3)

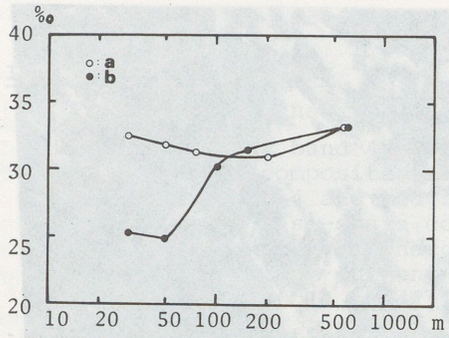

Fig.3 Relationships between salinity and sea depth at sites a and b (See Fig.2)

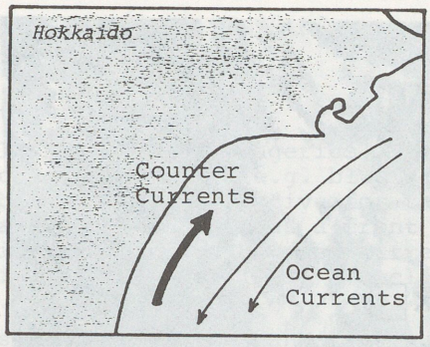

Fig.5 Ocean currents and counter currents off eastern Hokkaido

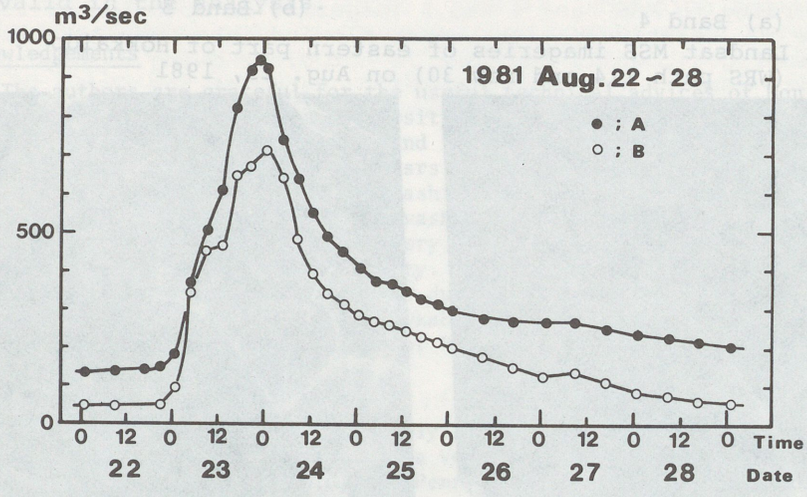

Fig.4 Water volume variation of the Tokachi River at sites A and B (See Fig.2)

(a) Aug.25, 1981 — Band 4

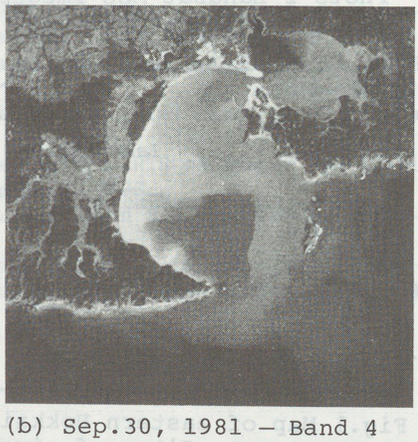

(b) Sep.30, 1981 — Band 4

Photo 3 Feature Variations of bay current in Akkeshi Bay (Indicated with T in Photo 1) and water pattern in Lake Akkeshi (Indicated with S in Photo 1 also)

(c) Oct

(e) Fe

Photo 3 Fea wit cat

Photo 4 La of

(c) Oct.4, 1980 — Band 4

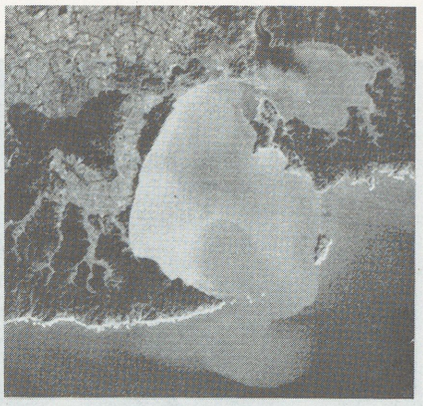

(d) Nov.5, 1981 — Band 4

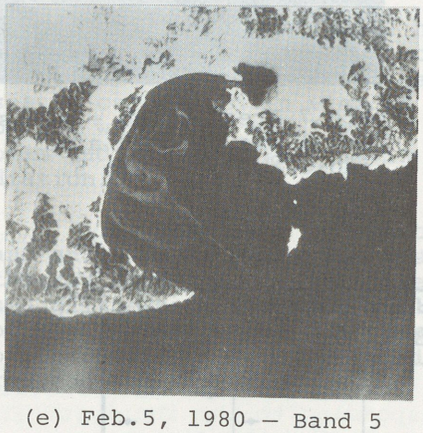

(e) Feb.5, 1980 — Band 5

(f) Feb.22, 1890 — Band 5

Photo 3 Feature Variations of bay current in Akkeshi Bay (Indicated with T in Photo 1) and water pattern in Lake Akkeshi (Indicated with S in Photo 1 also)

Photo 4 Landsat MSS band-5 imagery of site X in Photo 1

Photo 5 Landsat MSS band-5 & -7 imagery of site Y in Photo 1 — Sites 1 through 5 are flooded area reconized.

Photo 6 Areal photo – Sites 1 through 3 are flooded area indicated in Photo 5.

Photo 7 Areal photo – Sites 4 and 5 are flooded area indicated in Photo 5.

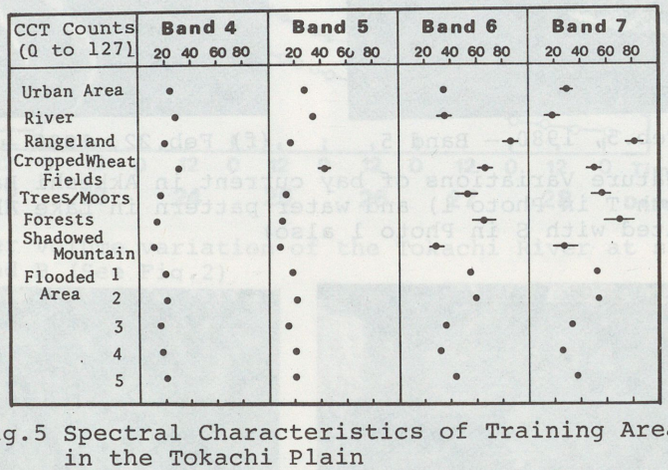

Fig.5 Spectral Characteristics of Training Area in the Tokachi Plain

Note: Flooded area 1 through 5 are indicated in Photo 5.

ON ANGULAR DISTRIBUTION OF RADIATION REFLECTED FROM A RUFFLED SEA

H. ARST

Institute of Thermophysics and Electrophysics
Estonian Academy of Sciences
Paldiski Str.1. Tallinn 200031
Estonian SSR , USSR

ABSTRACT

A mathematical model has been developed for describing the angular distribution of monochromatic electromagnetic radiation reflected from the ruffled sea surface. The reflectivity of the sea is calculated in view of the possibility of a thin oil film on the water.The model works both in case of an incident parallel beam radiation as well as in case of diffuse and direct solar radiation.

The model may become of practical use for the interpretation and analysis of measuring results of upwelling radiation above the sea surface (to estimate the relative contribution of the sun glitter and directly reflected sky radiation to the results of the measured sea brightness , to find the optimum directions of observations for determining the zones with increased or reduced sea radiance etc.).

The upwelling solar radiance above the sea surface consists of two components: 1)the sun and sky radiation directly reflected from water surface 2) solar radiation diffusely backscattered by seawater . An extensive and profound investigation on the radiance distribution over a ruffled sea has been made by G.N. Plass with co-authors using the Monte Carlo method (Plass et al. 1975, 1976, 1977, 1981, Guinn et al. 1979). However, we need a simple mathematical model describing the field of upwelling radiance above the sea in order to analyze and verify our experimental results (measurings have been carried out on board of a research vessel or helicopter). The computer of the research vessel must be able to realize the program of the mathematical model.

As a first step, a simple mathematical model for calculating the electromagnetic radiation directly reflected from the sea surface is developed. The model works both in case of an incident parallel beam radiation as well as in case of the diffuse and direct solar radiation. It describes reflected radiance measured by fictitious receiver as a function of the zenith angle (ϑ_m) and azimuth (α_m) of observation. The distorting influence of the atmosphere between the receiver and reflective surface is not taken into account. Nevertheless, in cases of small distances between the receiver and sea surface (vessel, helicopter) estimations made by this model could be satisfactory enough.

It is known that the reflected component of solar radiation B_R :

$$B_R(\alpha_m, \vartheta_m) = B(\alpha, \vartheta) R(\varphi_{nm}, x_0, x_1 \dots x_i), \quad (1)$$

where $B(\alpha, \vartheta)$ -sky brightness in the direction of ϑ (zenith angle) and α (azimuth), R -reflectivity of a surface element of the wind-ruffled sea, φ_{nm} -angle between the normal of wave surface element and the direction of incident beam, $x_0, x_1 \dots x_i$ -parameters characterizing optical properties of the sea surface under consideration.

Due to the dynamic character of the wind-ruffled sea, the determination of the unique value of the radiation reflected from a fixed surface element of water is quite out of question. Unregularity of real waves necessitate to use the probability functions to characterize the process of reflection from the rough sea surface. The reflected component of upward radiance is considered a weighted average, the probability of reflection from a given solid angle being a weight ratio. The reflecting wave surface is described by the probability law providing us the distribution of the normals of wave surface elements. Hence, we have

$$dB_R = B(\alpha, \vartheta) R(\varphi_{nm}, x_0, x_1 \dots x_i) P(\alpha_n, \vartheta_n) d\omega^*, \quad (2)$$

where $$d\omega^* = \frac{d\omega}{4 \cos \varphi_{nm}} = \frac{\sin \vartheta \, d\vartheta \, d\alpha}{4 \cos \varphi_{nm}} . \quad (3)$$

Here α_n and ϑ_n -correspondingly the azimuth and zenith angle of the normal of wave surface element, $P(\alpha_n, \vartheta_n)$ -the function characterizing the probability of direction of this normal, $2\varphi_{nm}$ - angle between the direction of observation (α_m, ϑ_m) and the variable direction (α, ϑ), $d\omega$ -solid angle of the sky surface element corresponding to the incident radiance $B(\alpha, \vartheta)$, $d\omega^*$ -solid angle for the direction of normal (α_n, ϑ_n) corresponding to the solid angle of incident radiation $d\omega$.

An incident beam could be both the direct solar and sky radiation. Hence,

$$B(\alpha, \vartheta) = B_o(\alpha_o, \vartheta_o) + B_s(\alpha, \vartheta), \quad (4)$$

where $B_s(\alpha, \vartheta)$ -brightness of the sky, $B_o(\alpha_o, \vartheta_o)$-brightness of the visible Sun's disc, α_o and ϑ_o -correspondingly the azimuth and zenith angle of the centre of Sun's disc. However, it's better to use not B_o , but the value of direct solar radiation flux onto a horizontal surface (E_o), which data is more available. As it is known , approximately

$$B_o \approx \frac{E_o}{\cos \vartheta_o \, \omega_o} , \quad (5)$$

where ω_o -solid angle of the visible Sun's disc.

Taking into account the various directions of wave surface normals, we obtain

$$\bar{B}_R = \int_0^{2\pi} \int_0^{\pi/2} B_s(\alpha, \vartheta) R(\varphi_{nm}, x_0, x_1 \dots x_i) P(\alpha_n, \vartheta_n) \frac{\sin \vartheta}{4 \cos \varphi_{nm}} \, d\vartheta \, d\alpha + \quad (6)$$

$$+ \frac{E_o R(\varphi_{mno}, x_0 \dots x_i) P(\alpha_{no}, \vartheta_{no})}{4 \cos \vartheta_o \cos \varphi_{nmo}} .$$

Here $2\varphi_{nmo}$ -angle between the directions of observation and the sun, α_{no} and ϑ_{no} - correspondingly the azimuth and zenith angle of the normal of sea surface element in case of the incident direct solar radiation. Both α_n and ϑ_n are calculated as the azimuth and zenith angle of the bisectrix of the angle between the directions of (α_m, ϑ_m) and (α, ϑ). In case of the direct radiation , α_{no} and ϑ_{no} are calculated for the bisectrix of the angle between (α_m, ϑ_m) and (α_o, ϑ_o).

The first term of the formula (6) describes the reflected sky radiance, the second the sun glitter.

Evidently the data on B_s as a function of α and ϑ for various Sun's locations is needed. Practically, in most cases, we have the experimental results of total solar and sky irradiance, but not the angular distribution of $B_s(\alpha, \vartheta)$. For the first approximation we took the sky radiance as subjected to the following assumptions: 1) the maximum value of B_s corresponds to the direction of the visible Sun's disc: 2) the sky radiance decreases continuously with the direction (α, ϑ) moving away from the sun's direction. Under these restrictions the angular distribution of $B_s(\alpha, \vartheta)$ can be described mathematically by an ellipsoid assuming the longer axis of symmetry directed straight to the Sun's disc. For our model such a function $B_s(\alpha, \vartheta)$ was determined for absolutely clear (for various sun's heights) and completely cloudy sky. It must be pointed out that one way to improve our mathematical model is to obtain more perfect description of $B_s(\alpha, \vartheta)$.

The values of reflectivity $R(\varphi_{nm}, x_o \ldots)$ both for the cases of pure water and a thin oil film on the sea surface are computed by the formulae presented by Arst, Kard (1981) while using the optical constants of water and oil taken from the investigations of Irvine, Pollack (1968) and Zolotariev et al. (1977).

For determining the function $P(\alpha_n, \vartheta_n)$, the results of the investigation by Guinn et al. (1979) are very convenient: on the basis of the data of Cox and Munk (1954) they have presented the formulae for calculations of $P(\alpha_n, \vartheta_n)$ as well as the necessary expressions for computational parameters (both for pure water and oil slick). The expressions are developed in the form that depends only on the velocity and direction of the wind. Those characteristics are easily available. We have used these formulae for computing the values of $P(\alpha_n, \vartheta_n)$ and $P(\alpha_{no}, \vartheta_{no})$.

The given model is realized as a program for a computer. The initial data is: 1) wavelength of incident radiation; 2) solar zenith angle and azimuth; 3) zenith angle of observation (the azimuth of observation is considered to be zero); 4) thickness of oil film; 5) optical constants of water and oil; 6) wind velocity and direction; 7) downwelling total and direct solar irradiance measured on the sea surface. (It is possible to refine the results, having some measured values of sky brightness as initial data that help to determine the function $B_s(\alpha, \vartheta)$ for the case under consideration). The results of the program's single run are the values of the upwelling reflected radiance, separately for the reflected sky radiation and sun glitter (both for the calm and ruffled sea with and without oil film covering).

The model may become of practical use for the analysis of measuring results of upward radiation above the sea. One of the possible applications can be the estimation of relative contribution of the sun glitter to the results of the

measured sea radiance. Besides, the model enables to establish the optima directions of observation in determining the zones with increased or reduced (compared to the surrounding sea surface) sea radiance for the given observation conditions (the Sun's position, wind velocity and direction, cloudiness). The above zones of different (increased or reduced) brightness may result from the oil film , variation of sea roughness under the influence of internal waves etc.

We have carried out the computations by the given model for the incident solar radiation wavelength of 0.7 microns .It must be marked that for the wavelengths approximately 0.7 microns and more the diffusely backscattered (from water) component of upward radiation is negligible. Hence, for these wavelengths the reflecting component represents practically the sea brightness.

In the calculations the relationship between the sea brightness and the observation conditions (the observation direction, the solar zenith angle and azimuth, the wind velocity and direction) is considered.

Since we had no initial data of total and direct solar radiation for all cases under consideration and no data at all to determine the B_s as a function of α and Ω ,we used the averaged data for the values of the relationship between the direct and total solar radiation as well as for the values of the angular distribution of sky brightness taken from handbooks (see Kondratiev (1954),Ivanoff (1978),Avaste et al.(1962)). By means of these materials the relative values of B_s and E_o were determined and also the parameters of the ellipsoid describing the angular distribution of $B_s(\alpha, \vartheta)$.As a result, we have by now the values of $\bar{B}_R$ only in relative units.

Some examples of our results are demonstrated below. Fig.1 and 2 represent the variability of sea brightness according to the change of the solar zenith angle (ϑ_o) and the wind velocity (w) (both for pure and for oil slick covered water). A significant difference in results of $\bar{B}_R$ is observed. One can see that in certain conditions anomalous contrasts may appear - brightness of clear water exceeds the corresponding values of the system "oil film-water". Fig.3 enables to estimate the contribution of sun glitter to the sea brightness. As seen, the maximum values of glitter occur for solar azimuth angles being approximately 180^0 and apparently the opposite direction is more recommended for measurements where the influence of sun glitter must be minimized. It is established too that for avoiding the influence of sun glitter, the nadir direction of measurements is not suitable, but the directions of ϑ_m being about $40 \div 50^o$ must be preferred (the same conclusion is presented in the papers of Plass et al.(1977)).

In Fig.4 we can see the scanning curves of $\bar{B}_R$(zenith angle ϑ_m changing from 20^o to 50^o) with the assumption that in the zone of ϑ_m from 26^o to 34^o the water is covered with oil slick. We found that the shapes of the brightness curves as well as the contrasts between the values of $\bar{B}_R$ with and without oil film on water depend significanly on the solar azimuth angle.

Our results show likewise the dependence of $\bar{B}_R$ on the wind direction. It means that in spite of the stochastic character of the sea roughness the certain slopes of waves dominate. This dependence is not so strong for oil-covered sea: hence, the waves are more symmetrical under these conditions.

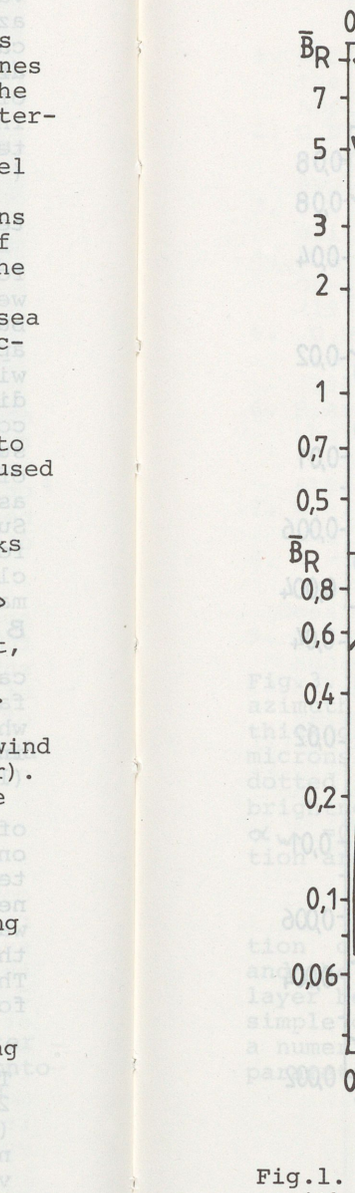

Fig.1.
zenith
angle
microns
microns
angles
w

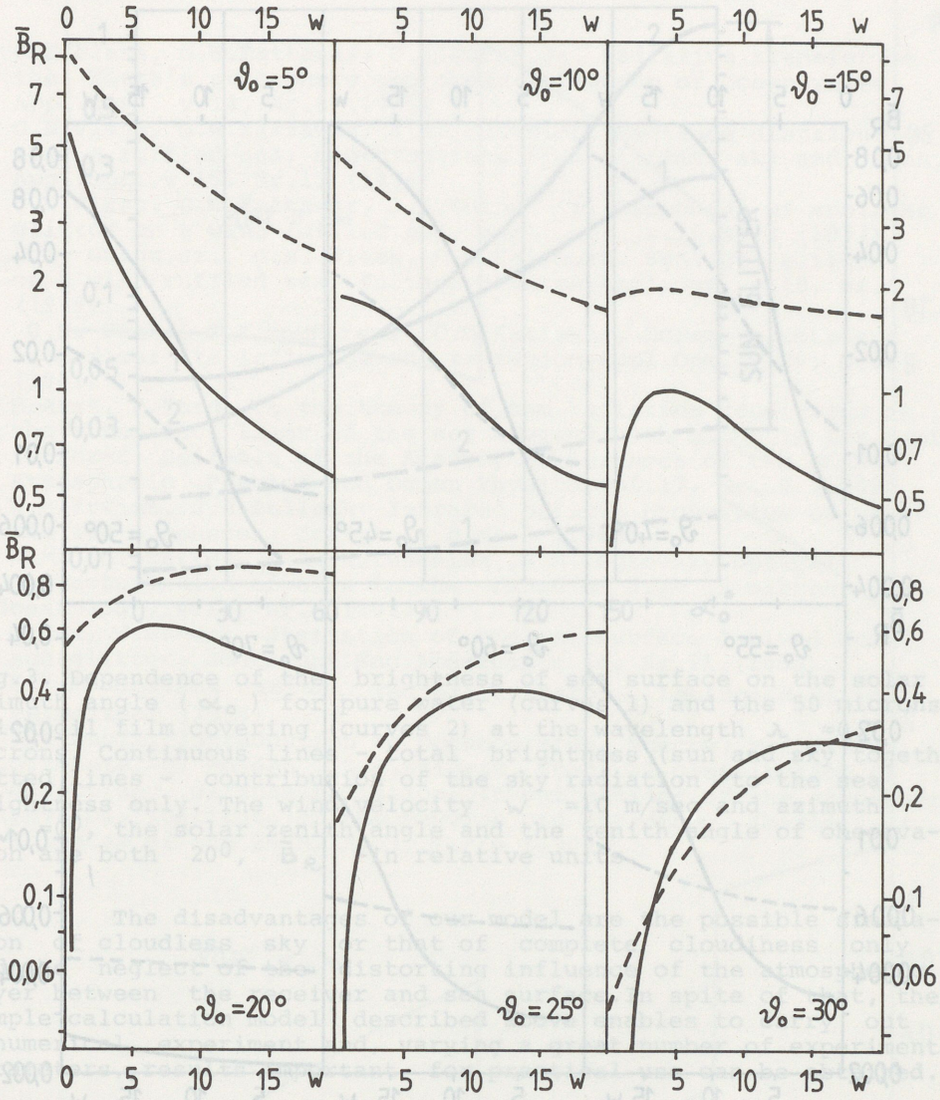

Fig.1. Dependence of the brightness of sea surface on the solar zenith angle (ϑ_o) and on the wind velocity (W) for the zenith angle of the observation $\vartheta_m = 0$ and at wavelength λ =0.7 microns. Continuous lines - for pure water, dotted lines - for 50 microns thick oil film on the water. The wind and solar azimuth angles are equal. The $\bar{B}_R$ values are in relative units, the W values in m/sec.

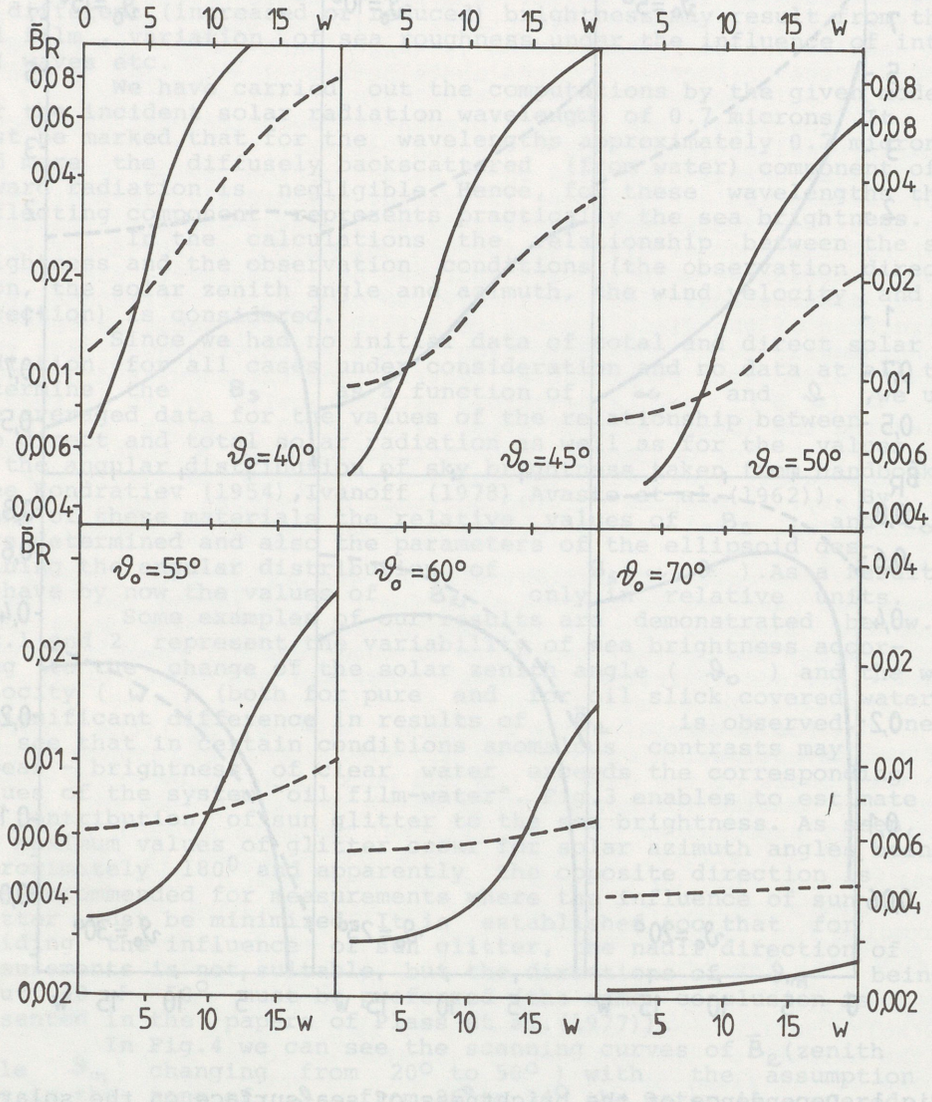

Fig.2. Dependence of the brightness of sea surface on the solar zenith angle and on the wind velocity for ϑ_m =0 and λ =0.7 microns. The symbols and units are the same as in Fig.1.

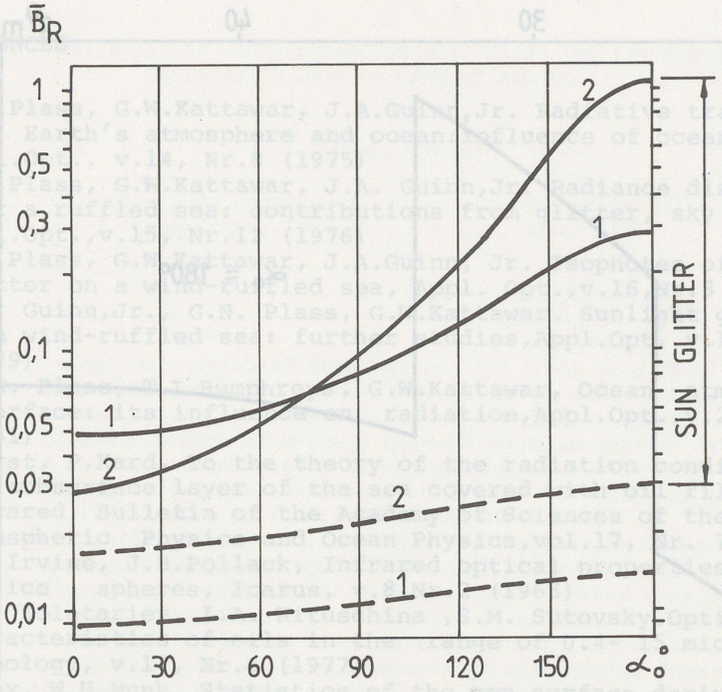

Fig.3. Dependence of the brightness of sea surface on the solar azimuth angle (α_0) for pure water (curves 1) and the 50 microns thick oil film covering (curves 2) at the wavelength λ =0.7 microns. Continuous lines - total brightness (sun and sky together), dotted lines - contribution of the sky radiation to the sea brightness only. The wind velocity W =10 m/sec and azimuth α_W =0^0, the solar zenith angle and the zenith angle of observation are both 20^0, $\bar{B}_R$ -in relative units.

The disadvantages of our model are the possible simulation of cloudless sky or that of complete cloudiness only and the neglect of the distorting influence of the atmospheric layer between the receiver and sea surface.In spite of that, the simple calculation model described above enables to carry out a numerical experiment and, varying a great number of experimental parameters, results important for practical use can be obtained.

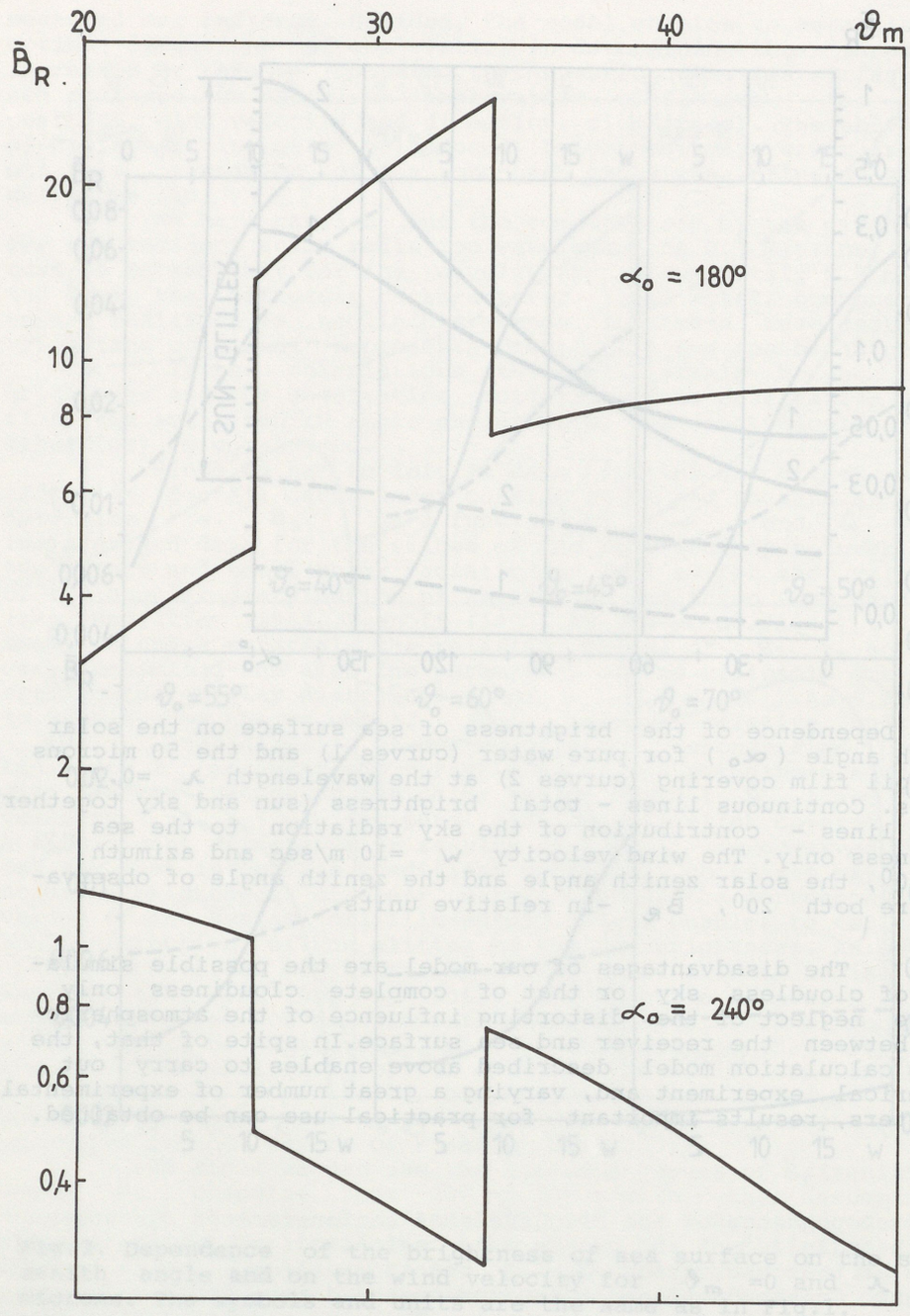

Fig.4. Dependence of the brightness of the sea surface on the zenith angle of observation (ϑ_m) at λ =0.7 microns assuming that only in the zone of $24^0 \leq \vartheta_m \leq 36^0$ the water is covered with 50 microns thick oil film. The solar azimuth angle is shown near both curves. The wind velocity W =10 m/sec and azimuth α_w =90°, $\bar{B}_R$ - in relative units.

REFERE

1. G.N.
the
Appl
2. G.N.
over
Appl
3. G.N.
glit
4. J.A.
on a
(197
5. G.N
inte
(198
6. H.Ar
the
infr
Atmo
7. W.M.
and
8. W.M.
chara
Oceano
9. C.Cox
sun
10. K.Y.
mete
11. A.Iv
12. O.Av
direc
phys
Scie

REFERENCES

1. G.N.Plass, G.W.Kattawar, J.A.Guinn,Jr. Radiative transfer in the Earth's atmosphere and ocean:influence of ocean waves, Appl.Opt., v.14, Nr.8 (1975)
2. G.N.Plass, G.W.Kattawar, J.A. Guinn,Jr. Radiance distribution over a ruffled sea: contributions from glitter, sky and ocean, Appl.Opt.,v.15, Nr.12 (1976)
3. G.N.Plass, G.W.Kattawar, J.A.Guinn, Jr. Isophotes of sunlight glitter on a wind-ruffled sea, Appl. Opt.,v.16,Nr.3 (1977)
4. J.A. Guinn,Jr., G.N. Plass, G.W.Kattawar. Sunlight glitter on a wind-ruffled sea: further studies,Appl.Opt.,v.18, Nr.6 (1979)
5. G.N. Plass, T.I.Humphreys, G.W.Kattawar, Ocean -atmosphere interface: its influence on radiation,Appl.Opt.,v.20, Nr.6 (1981)
6. H.Arst, P.Kard, To the theory of the radiation conditions in the subsurface layer of the sea covered with oil film for near infrared, Bulletin of the Academy of Sciences of the ESSR, Atmospheric Physics and Ocean Physics,vol.17, Nr. 7 (1981)
7. W.M.Irvine, J.B.Pollack, Infrared optical properties of water and ice spheres, Icarus, v.8,Nr.2 (1968)
8. W.M. Zolotariev, I.A. Kituschina ,S.M. Sutovsky.Optical characteristics of oils in the range of 0.4- 15 microns. Oceanology, v.17, Nr.6 (1977)
9. C.Cox, W.H.Munk, Statistics of the sea surface derived from sun glitter, Journ.Opt.Soc.America, v.44, Nr.11 (1954)
10. K.Y.Kondratiev, Solar radiation energy , Leningrad,Gidrometeoizdat (1954).
11. A.Ivanoff, Intruduction to Oceanography, Moscow, Mir (1978).
12. O.Avaste, H. Moldau , K.S.Shifrin, Spectral distribution of direct and diffuse radiation, Investigations of the atmospheric physics, Institute of the Physics and Astronomy, Academy of Sciences of the ESSR, No.3, Tartu (1962).

ABSTRACT

Using
due to the
some coast
combinatio
estimation
is consist
correction
From
and sea su
indicates
population
polution i
water orig
under the
is carried
data.

INTRODUCTI

Since
become ava
MSS data t
and the au
informatio
The Earth
started it
monitoring
increased
inclining
Due t
the analys
coastal ar
of view of
data is ce
areas.
Althou
meteorolog
i.e. sea su
has an adva
area twice
great disad
Thus
that of NOA
be great he
areas.
In thi
results of
synchronous